JOURNAL OF AIRCRAFT
Vol. 44, No. 3, May–June 2007

Dynamic Wing Airloads with Higher Harmonic Flap Motion

P. Gerontakos* and T. Lee†
McGill University, Montreal, Quebec H3A 2K6, Canada

DOI: 10.2514/1.26323

The effect of higher harmonic flap motion (actuated at selected start times t_s and amplitudes $\delta_{\max}$) on the dynamic-load loops of an oscillating NACA 0015 wing was investigated. At fixed t_s and $\delta_{\max}$, the 2P or 2/rev flap motion led to a significant alleviation of the nose-down pitching-moment coefficient C_m and the negative torsional damping, compared with a wing with and without 3P and 4P flap control. The 3P flap motion always provided an improved negative peak C_m, accompanied by a slightly increased maximum lift coefficient $C_{l,\max}$ and a virtually unchanged net torsional damping, regardless of t_s, compared with 4P flap control. The results also show that the later the 2P flap actuation, the higher the net torsional damping and nose-down pitching moment. The 4P flap motion always rendered a reduced $C_{l,\max}$, regardless of t_s and $\delta_{\max}$.

Nomenclature

C_d	=	section drag coefficient
C_l	=	section lift coefficient
C_m	=	section pitching-moment coefficient
$C_{m,\text{peak}}$	=	peak C_m
C_p	=	surface pressure coefficient
C_w	=	torsional damping factor
$C_{w,\text{cw}}$	=	clockwise or negative C_w
$C_{w,\text{ccw}}$	=	counterclockwise or positive C_w
$C_{w,\text{net}}$	=	net C_w value, $C_{w,\text{ccw}} + C_{w,\text{cw}}$
c	=	airfoil chord
f_o	=	oscillation frequency
NP	=	nth harmonic of f_o
P	=	per revolution
Re	=	Reynolds number, $u_o c/\nu$
t	=	time
t_d	=	flap actuation duration
t_s	=	flap actuation start time
t_{ss}	=	steady-state time period
u, v	=	mean axial and transverse velocity
u', v'	=	streamwise and transverse velocity fluctuation
u_o	=	freestream velocity
x, y, z	=	streamwise, transverse, and spanwise distances
α	=	angle of attack
α_m	=	mean angle of attack
$\alpha_{\max}$	=	maximum angle of attack
$\alpha_{\min}$	=	minimum angle of attack
α_{ss}	=	static-stall angle
$\Delta\alpha$	=	oscillation amplitude
ΔC_l	=	$C_{l,\text{controlled}} - C_{l,\text{baseline wing}}$
$\delta_{\max}$	=	peak-to-peak flap deflection
κ	=	reduced frequency, $\pi f_o c/u_o$
ν	=	kinematic viscosity

Subscripts

d	=	pitch-down
u	=	pitch-up

Received 4 July 2006; revision received 28 November 2006; accepted for publication 30 November 2006.

*Graduate Research Assistant, Department of Mechanical Engineering.
†Associate Professor, Department of Mechanical Engineering. Member AIAA

I. Introduction

THE dynamic overshoots in lift force and the accompanied high torsional and pitch control loads on retreating rotor blades continue to make dynamic stall and its control an important topic in rotorcraft engineering. The dynamic-stall flow phenomena are characterized by the upstream progression of the flow reversal and the subsequent formation, convection, and spillage of an energetic leading-edge vortex (LEV) over the wing upper surface, which induces a nonlinearly fluctuating pressure field and produces large transient variations in forces and nose-down pitching moments that may be many times larger than their static counterparts. During poststall, the flow process is characterized by a large hysteresis in the dynamic aerodynamic load loops and the presence of large nose-down pitching moments, which leads to a substantial increase in blade torsional loads and is the main adverse characteristic of dynamic stall that concerns the helicopter dynamicists. An excellent review of unsteady airfoils is given by McCroskey [1].

A number of passive and active dynamic-stall flow control means (through the use of trailing-edge flaps [2–6], pulsating and synthetic jets [7,8], leading-edge blowing and suction [9], dynamically deformable leading edges [10], etc.) have been proposed to minimize or eliminate the large hysteresis in the nonlinear airloads and the detrimental negative aerodynamic damping. Among them, the trailing-edge flap (TEF) flow control has been considered extensively by researchers to control the large negative damping or nose-down pitching moment induced on unsteady wings undergoing dynamic-stall oscillations, as well as for the control of the unsteady lift (including flutter suppression and gust alleviation). A representative numerical simulation of the TEF control of the pitching-moment loads associated with the dynamic stall occurring on a NACA 0012 airfoil [oscillated with $\alpha(t) = 15\,\text{deg} + 10\,\text{deg}\sin\omega t$ and a reduced frequency of 0.173 with $Re = 1.463 \times 10^6$] was performed by Feszty et al. [5]. They found that the nose-down pitching moment could be reduced by the use of an optimum pulsed trailing-edge flap (of 16% chord) motion, represented by $\delta(t) = \delta_{\max}[1 - \cos(t/t_d)]$, with an upward flap deflection of $\delta_{\max} = 20\,\text{deg}$ and a flap duration of about one-third of the airfoil motion time period. Moreover, the trailing-edge vortex, induced by the downstream convecting LEV, was found to be responsible for the large negative pitch moment and the associated negative damping. The surface pressure distributions were, however, not reported.

The detailed surface pressure measurements of a NACA 0015 wing equipped with a dynamically deflecting 25% chord flap [oscillated with $\alpha(t) = 15\,\text{deg} + 10\,\text{deg}\sin\omega t$ and $\kappa = 0.05$ at $Re = 1.65 \times 10^5$] were documented recently by Gerontakos and Lee [6]. Similar to the pulsed flap motion employed by Feszty et al. [5], the first-harmonic TEF actuation consisted of a brief pulse, represented by a constant ramp-up motion, remained steady briefly, and was followed by a constant ramp-down motion (Fig. 1c). The

prescheduled TEF motions were actuated at start times $t_s = -0.5, 0,$ and 0.5π (corresponding to a flap actuation at $\alpha_{\min}$, α_m, and $\alpha_{\max}$, respectively), with $\delta_{\max} = \pm 7.5$ and ± 15 deg and $t_d = 0.35$ to 50% f_o^{-1}. Gerontakos and Lee summarized that

1) The larger the upward $\delta_{\max}$, the more efficient the negative $C_{m,\text{peak}}$ reduction mechanism.

2) The shorter the t_d, the smaller the poststall lift loss.

3) The magnitudes of maximum C_l and C_d seemed to be somewhat insensitive to the extent of flap actuation duration, but were of lower values than a baseline, or uncontrolled, wing.

4) The later the t_s, the larger the net torsional damping factor, in general.

5) The leading-edge-vortex formation and detachment were not affected by the TEF motion, whereas the low-pressure signature or footprint of the LEV was, however, reduced by the upward flap deflection. More important, the reduction in $|-C_{m,\text{peak}}|$ was found to be mainly a consequence of the suction pressure introduced on the lower surface of the control flap. In conclusion, a relatively early upward flap actuation with $\delta_{\max} \geq 60\%\alpha_{\max}$ (initiated between α_{ss} and $\alpha_{\max}$ during pitch-up) and a t_d of about 50% of the oscillation cycle time was found to be most effective in reducing the nose-down pitching-moment excursion and in providing a good compromise between negative damping reduction and dynamic lift maximization.

In addition, it is noteworthy that for a conventional helicopter, the lack of smoothness (as a result of the variation of local velocity and blade angle of attack) caused by effects other than the swashplate introduced smooth cyclic pitch could eventually result in vibration. Various active control schemes such as active pitch link, higher harmonic control, trailing-edge flap control, spoilers, and individual blade control have been proposed to reduce the vibration levels by modifying the periodic aerodynamic loads such that they no longer produce the detrimental effects. Among them, higher harmonic control (HHC) [11–17] has received increasing attention over the last two decades, especially as a means of alleviating vibratory loads and

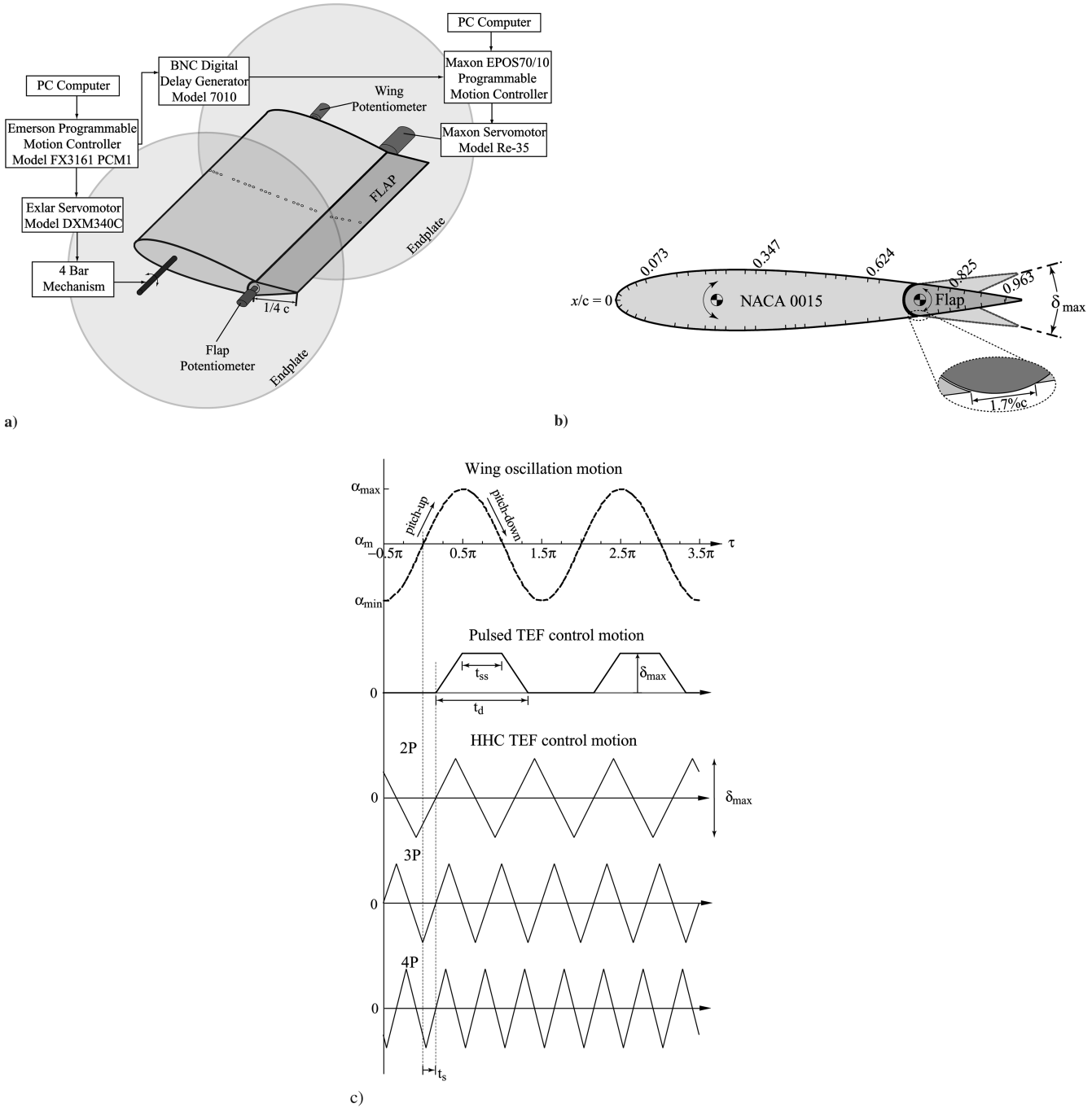

Fig. 1 Schematics of oscillation wing model and experimental setup, surface pressure tap locations, and pulsed and HHC flap motions and definitions.

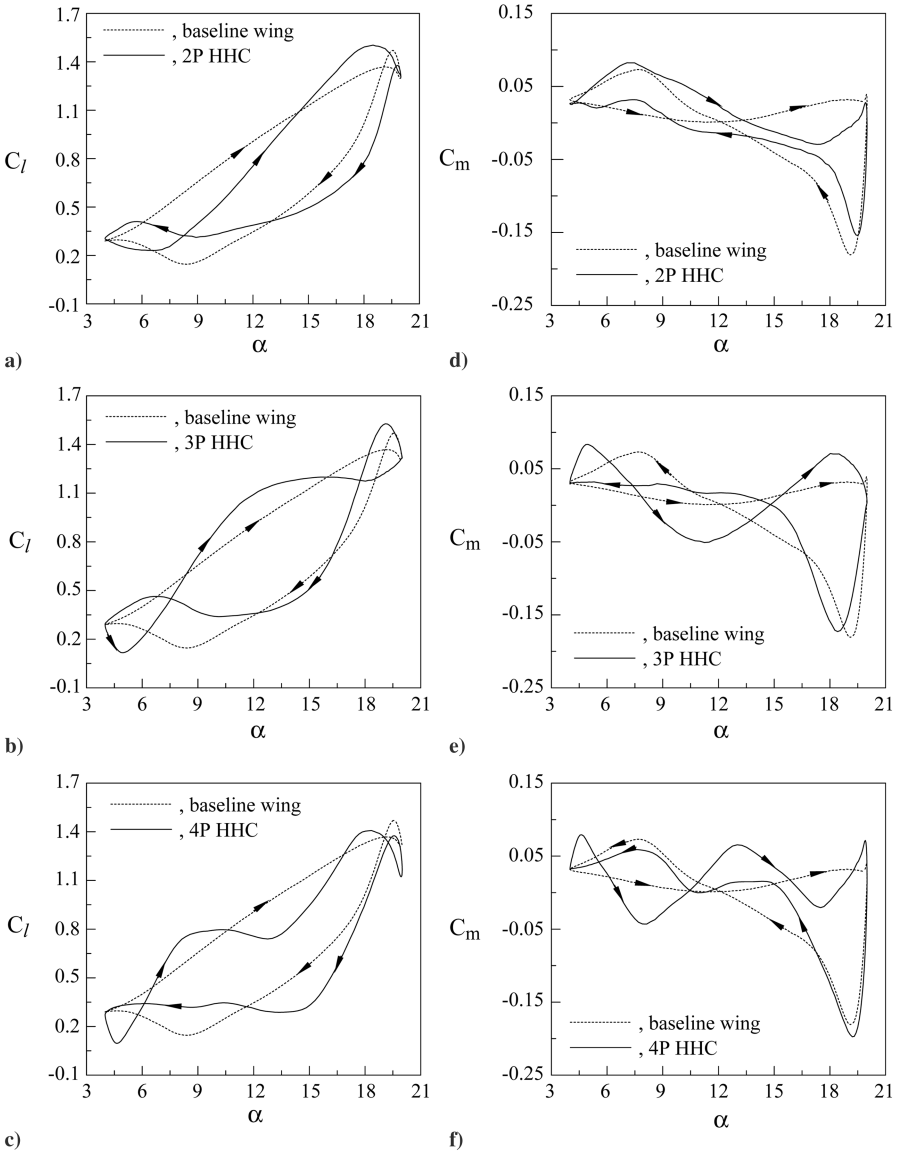

Fig. 2 Effect of HHC flap motion on dynamic-load loops with $t_s \approx -0.5\pi$ and $\delta_{max} = 16$ deg.

reducing blade-vortex interaction (BVI) noise by modifying the rotor blade pitch at harmonic frequencies above the rotor rotational frequency. The pioneering analytical study was first performed by Payne [11], who showed the potential effectiveness of HHC in alleviating retreating blade stall. Extensive research on the use of HHC implemented in the form of individual blade control was carried out by Ham [12] and his coworkers. Enenkl et al. [17] suggested that the way an active trailing-edge servo-tab reduces noise and vibration may vary, depending mainly on flap chord, control frequency, and the blade's torsional stiffness. No detailed dynamic-load distributions on the wing, however, were reported.

The objective of this study was to investigate the effect of HHC flap motion on the dynamic-load loops of an oscillating NACA 0015 wing. Detailed phase-locked ensemble-averaged surface pressure distributions, supplemented by cross-hot-wire wake flow measurements, were obtained to quantify the prescheduled HHC flap control schemes. Special emphasis was placed on the prescheduled HHC pitch inputs at two, three, and four times per revolution (i.e., 2P, 3P, and 4P) on the behavior of the unsteady C_l and C_m loops at selected TEF actuation start times and amplitudes. Physical mechanisms responsible for the affected changes were also discussed.

II. Experimental Methods

The experiment was conducted in a $0.9 \times 1.2 \times 2.7$ m suction-type wind tunnel at McGill University, with a freestream turbulence intensity of 0.03% at $u_o = 35$ m/s. A rectangular aluminum NACA 0015 airfoil with a chord length of 25.4 cm and a span b of 38 cm was used as the test model. The wing model was mounted horizontally at the center of the wind tunnel test section. The origins of the coordinates were located at the leading edge of the airfoil. The freestream velocity u_∞ was fixed at 15 m/s, which rendered a chord Reynolds number of 2.5×10^5. A specially designed four-bar oscillation mechanism, in conjunction with an Exlar model DXM340C servomotor driven by an Emerson model FX3161 PCM1 programmable motion controller, was used to oscillate the wing model with $\alpha(t) = 12\,\text{deg} + 8\,\text{deg}\sin\omega t$ and $\kappa = 0.1$ (Fig. 1a). The oscillation frequency was measured by the use of a potentiometer mounted on the servomotor shaft to an accuracy of ± 0.02 Hz. The four-bar mechanism provided an output that was sinusoidal to within 2%. The airfoil pitch axis was located at the quarter-chord location. The instantaneous angle of attack of the airfoil and the phase reference signal were recorded from a potentiometer mounted on the servomotor shaft. The surface pressure distributions were obtained from 48 0.35-mm-diam pressure taps, covering up to $x/c = 96.5\%$, distributed over the upper and lower surfaces of the wing model (Fig. 1b). The pressure signals were phase-locked ensemble-averaged over 100 cycles of oscillation and were integrated numerically to compute the unsteady aerodynamic loads and pitching moments. An uncertainty analysis gives a typical total uncertainty ± 0.013 in C_p. The wake of the airfoil model was

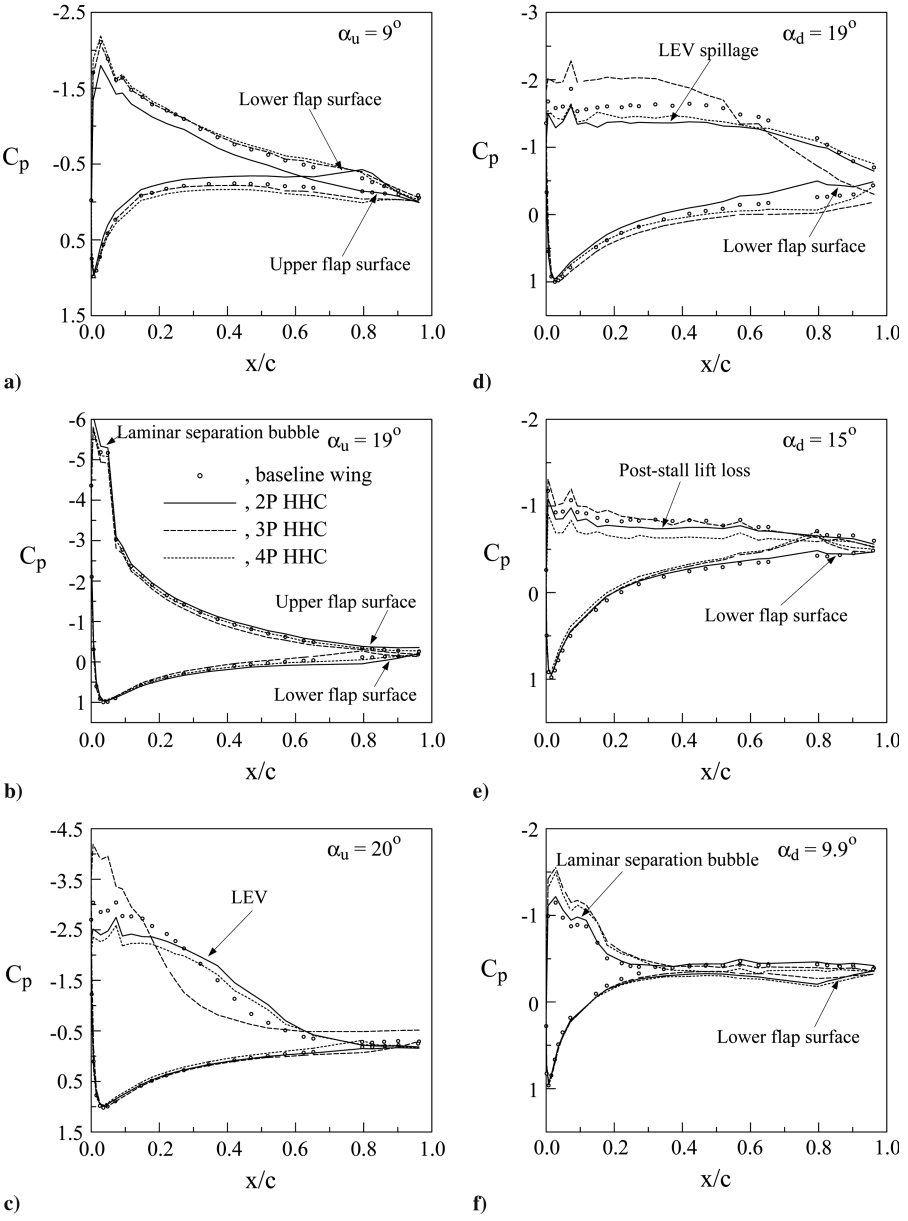

Fig. 3 Typical C_p distributions.

examined by using a miniature cross-hot-wire probe, located at $x/c = 1.75$, operated by two Dantec 56C17 constant-temperature anemometers. Details of the experimental setup are given by Gerontakos and Lee [6].

The wing model was equipped with a full-span trailing-edge flap (of 25% c), which was activated and deactivated independently by a Maxon servomotor (model Re-35), incorporating a 4.3:1 helical gearbox and an optical encoder. The flap motion, triggered in response to the oscillating wing phase angle τ, can be programmed into a series of sawtooth deflections. The time of TEF initial deflection (i.e., start time) and peak-to-peak deflection amplitude were determined by a Maxon EPOS 70/10 programmable motion controller. Flap deflections described by a HHC sawtooth waveform at 2P, 3P, and 4P of different t_s and $\delta_{\max}$ were employed in the present experiment (Fig. 1c). Note that this new servomotor TEF-control system was newly integrated to provide better TEF motion capability with improved accuracy, compared with the specially designed and constructed TEF-control system employed previously [6]. The flap actuation start time (between -0.5 and 0.2π, or $\alpha_{\min}$ and the angle of attack at which the LEV initiates) and $\delta_{\max}$ (8 and 16 deg) were tested to quantify their effects on the behavior of the dynamic C_l and C_m loops and on the wake flow structure. Note that when the phase angle was within the range $-0.5\pi \le \tau \le 0.5\pi$, the wing was described to be in pitch-up; when $0.5\pi \le \tau \le 1.5\pi$, the wing was said to be in pitch-down. Also, in the following discussion, the subscript u is used to indicate pitch-up when α is increasing and d is used to indicate pitch-down when α is decreasing.

III. Results and Discussion

A. Effect of NP

The influence of the higher harmonic flap motion (i.e., $NP = 2P$, 3P, and 4P), actuated at $t_s \approx -0.5\pi$ (i.e., $\alpha_u = \alpha_{\min}$ or, at the beginning of the pitch-up motion, with $\delta_{\max} = 16$ deg) on the dynamic C_l and C_m loops was examined first. The results were also compared with those of a baseline, or uncontrolled, wing. Figure 2a shows that for a 2P flap motion actuated at $t_s \approx -0.5\pi$, the C_l was reduced for $\alpha_u \approx \alpha_{\min}$ to α_m (or 4 to 12 deg) and increased for $\alpha_u = \alpha_m$ to $\alpha_{\max}$ (or 12 to 20 deg), as a result of the negative and positive camber effects (especially in the trailing region) induced by the upward and downward flap deflection as the wing was pitching up. During the wing pitch-down motion, the upward and downward flap motion was repeated: the C_l was first decreased (for $\alpha_d = \alpha_{\max}$ to α_m), with an increase in poststall lift loss (compared with a baseline

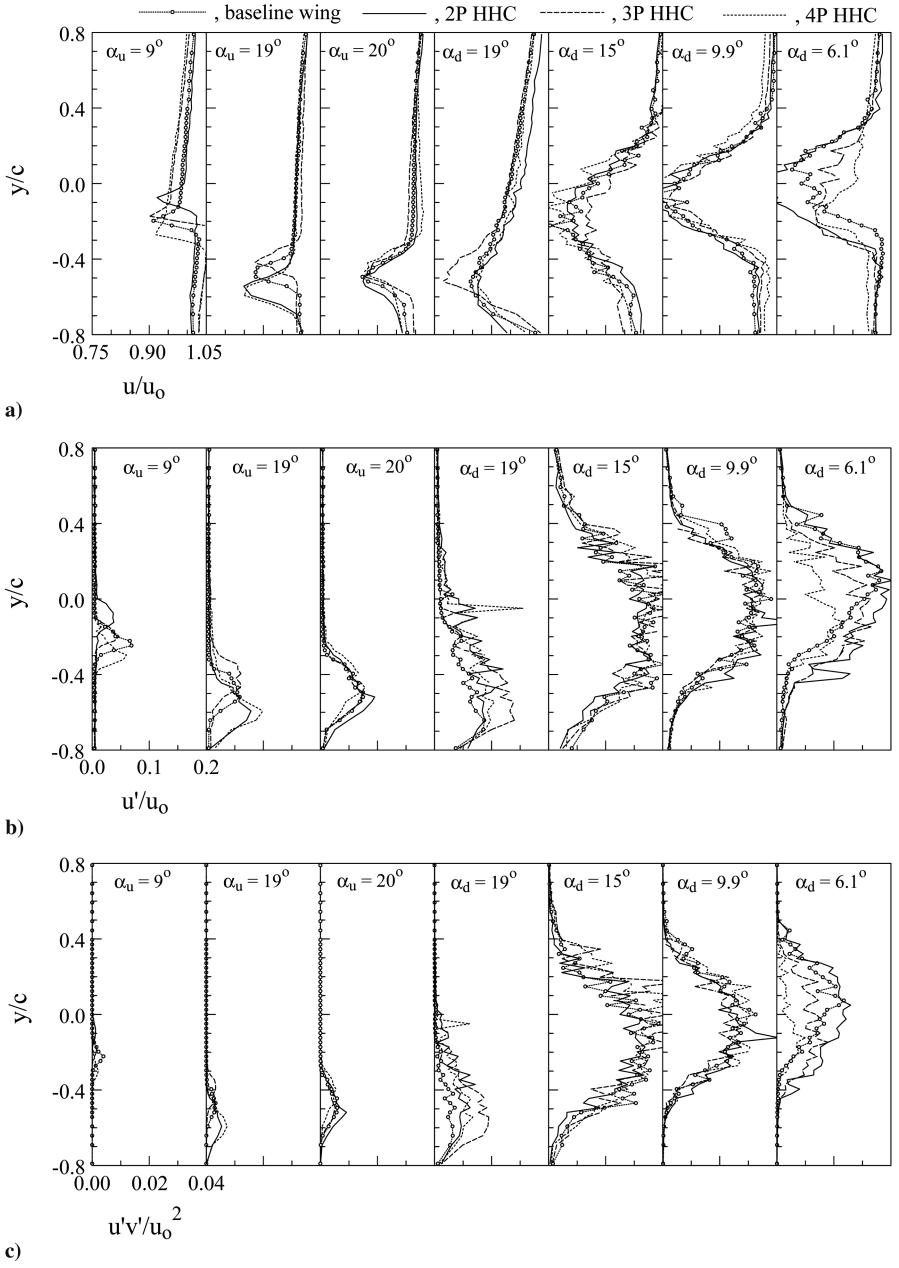

Fig. 4 Typical wake flow structures.

wing), and was followed by a somewhat promoted pitch-down flow reattachment and a subsequent increase in C_l. The physical mechanisms responsible for the observed increase and decrease in C_l can be illustrated from the detailed C_p distributions (Fig. 3) and the near-wake flow structures (Fig. 4). Figure 3a shows that at $\alpha_u = 9$ deg during the pitch-up attached-flow process, the upward flap motion led to an overall reduction in both suction and positive pressure pressures along the wing surfaces, compared with a baseline wing. Special attention should be given to the significant C_p reduction that appeared on both the lower and upper flap surfaces. The wake width and the shape of the wake profile remained unchanged (except for the upward shifting of the wake centerline; Fig. 4a), whereas u' (Fig. 4b) and Reynolds stress distributions (Fig. 4c) across the wake were slightly suppressed. Note that, in general, the upward TEF motion was efficient in containing a reduced momentum deficit throughout the oscillation cycle and resulted in reduced drag, wake width, and u'. At $\alpha_u = 19$ deg, the downward flap deflection rendered an advantageous pressure distribution, especially on both the upper and lower flap surfaces (Fig. 3b), and was accompanied by a slightly widened and downward-shifted wake, with enhanced u' and $u'v'$ (Fig. 4) across the wake, compared with a baseline wing.

The present C_p measurements also indicate that for a 2P HHC flap control with $t_s \approx -0.5\pi$ and $\delta_{\max} = 16$ deg, the initiation of the LEV was not affected by the downward-deflected flap (Figs. 3c and 4), whereas the "premature" spillage of the LEV was, however, delayed to $\alpha_d = 18.5$ deg (with $C_{l,\max} = 1.51$) during pitch-down (Figs. 2a, 3d, and 4), compared with $\alpha_d = 19.6$ deg (with $C_{l,\max} = 1.46$) of a baseline wing. During the poststall flow condition, the upward flap-induced reduction in C_p was evident (e.g., at $\alpha_d = 15$ deg; Fig. 3e). Note that although the upward flap motion (between $\alpha_d = \alpha_m$ to $\alpha_{\min}$) did not significantly promote the pitch-down flow reattachment, it did, however, provide an improved C_p distribution [especially on both the flap surfaces (Fig. 3f)] and a more energetic wake with increased u, u', and $u'v'$. More important, for a 2P flap control actuated at $t_s \approx -0.5\pi$, a single clockwise (CW) $C_m - \alpha$ loop (of $C_{w,\text{cw}} = C_{w,\text{net}} = -0.66$) was observed, in contrast to the figure-eight-like $C_m - \alpha$ loops of a baseline wing (with $C_{w,\text{ccw}} = 0.26$ and $C_{w,\text{cw}} = -0.68$), suggesting a substantially increased negative damping. The torsional damping factor C_w was defined by

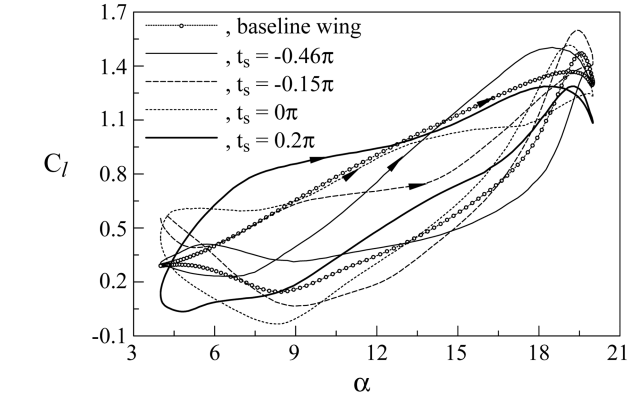

a)

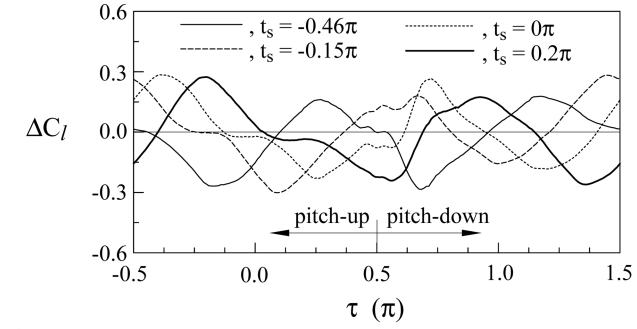

b)

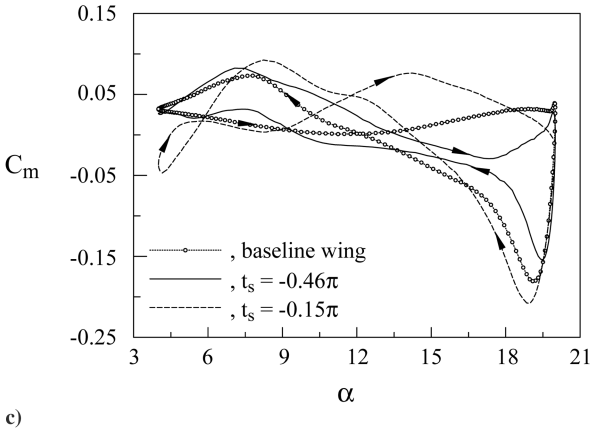

c)

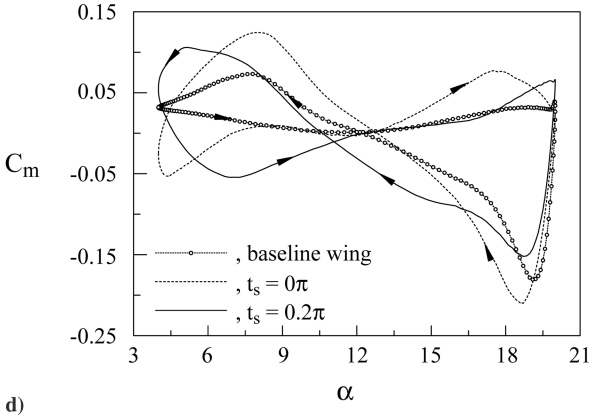

d)

Fig. 5 Effect of 2P flap motion on C_l, ΔC_l, and C_m.

the line integral of $C_m - \alpha$ loops and is positive when it corresponds to a counterclockwise (CCW) loop, whereas it is negative for a CW loop in the C_m versus α curve. The details of the HHC flap motion and the critical aerodynamic values are summarized in Table 1.

Figure 2b shows that for 3P flap control actuated at $t_s \approx -0.5\pi$, as expected, the observed decrease and increase in C_l was found to be consistent with the corresponding upward and downward flap motion; an increase in $C_{l,\max}$ (1.53 at $\alpha_d = 19.1$ deg) and a more evident promotion of the flow-reattachment process (compared with the 2P flap control case) can be clearly seen. The increase in $C_{l,\max}$, as a result of the small delay in the LEV initiation (of enhanced strength) and its spillage from the wing upper surface, can be demonstrated from the C_p distributions at a $\alpha_u = 20$ deg and $\alpha_d = 19$ deg (denoted by dashed lines in Figs. 3c and 3d) and from the wake flow measurements (Fig. 4). An increased wake deficit (u' and $u'v'$ at $\alpha_d = 19$ deg and $\alpha_d = 15$ deg) was observed, compared with a baseline wing with and without 2P flap control. The promotion of the flow reattachment (characterized by the reappearance of a laminar separation bubble in the leading-edge region; see, for example, Fig. 3f) near $\alpha_d = 9.7$ deg during pitch-down motion (compared with $\alpha_d = 8.3$ deg of a baseline wing) can also be seen from the C_p data. Furthermore, in addition to the observed C_l changes, an additional CW $C_m - \alpha$ loop was also observed, compared with a baseline wing; the net torsional damping $C_{w,\text{net}} = -0.43$, however, was found to remained unchanged, compared with a baseline wing (Table 1). That is, the rather drastic variation in C_l, induced by the 3P flap deflection, did not render any additional change in the net negative damping value or nose-down pitching-moment. A slightly reduced $|-C_{m,\text{peak}}|$ (compared with a baseline wing) was also exhibited (Table 1), although of much higher value than that of 2P flap control.

For an oscillating wing with 4P HHC flap control, an additional CW $C_m - \alpha$ loop (Fig. 2f), similar to the 3P flap control case (Fig. 2e), was also exhibited; the $C_{w,\text{net}}$ was not affected. A considerable increase in the peak negative pitching-moment coefficient $|-C_{m,\text{peak}}|$ was, however, observed. Also, other than the observed increase and decrease in C_l in response to the downward and upward flap deflections (Fig. 2c), the onset and the subsequent growth and spillage of the LEV was mainly unaffected (as indicated in Figs. 3c, 3d, and 4). In the meantime, the pitch-down flow reattachment (at $\alpha_d \approx 13.8$ deg) was found to occur much earlier, but more gradual, than a baseline wing. The flow-reattachment process was found to be characterized by basically unchanged u, u', and $u'v'$ distributions. A direct comparison of the effect of NP on the dynamic C_l, in terms of $\Delta C_l = C_{l,\text{HHC}}$ and $-C_{l,\text{baseline wing}}$, is presented in Sec. III.B.

In summary, the 2P flap deflection provided a significant alleviation of $-C_{m,\text{peak}}$ (or the large overshoot in nose-down pitching moment), whereas it provided a high $C_{w,\text{net}}$, compared with the 3P and 4P control cases and the baseline wing. The 3P flap motion rendered a reduced nose-down C_m, or $|-C_{m,\text{peak}}|$, a slightly increased $C_{l,\max}$, and a virtually unchanged $C_{w,\text{net}}$, compared with 4P flap control and a baseline wing. The 4P flap control provided the lowest $C_{l,\max}$ (below that of a baseline wing) and the highest $|-C_{m,\text{peak}}|$ among the three NP tested. Also, for all the HHC flap

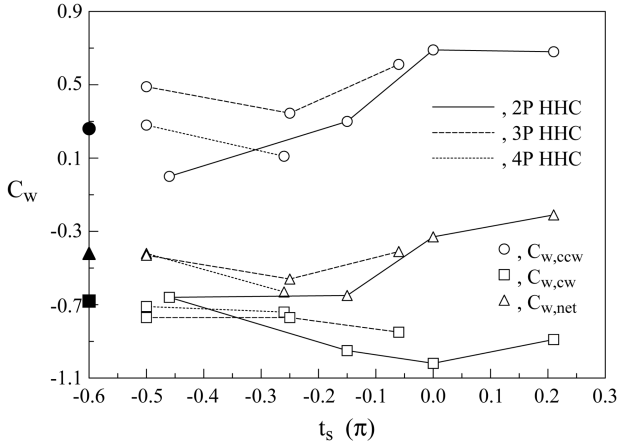

Fig. 6 Variation of C_w with t_s and *NP* for $\delta_{\max} = 16$ deg; solid symbols denote the baseline airfoil.

Table 1 TEF motion profile and critical aerodynamic values

	$\delta_{\max}$	t_s	$C_{l,\max}$	$\alpha\|_{C_{l,\max}}$ [a]	$-C_{m,\text{peak}}$	$\alpha\|_{C_{m,\text{peak}}}$ [a]	$C_{d,\max}$	$\alpha\|_{C_{d,\max}}$ [a]	$C_{w,\text{ccw}}$	$C_{w,\text{cw}}$	$C_{w,\text{net}}$
Baseline wing			1.46	19.6deg_d	0.181	19.1deg_d	0.50	19.4deg_d	0.26	−0.68	−0.42
2P	16 deg	-0.46π	1.51	18.5deg_d	0.154	19.5deg_d	0.46	19.7deg_d	0.00	−0.66	−0.66
2P	16 deg	-0.15π	1.60	19.4deg_d	0.208	19.0deg_d	0.53	19.2deg_d	0.30	−0.95	−0.65
2P	16 deg	0π	1.52	19.1deg_d	0.210	18.7deg_d	0.52	18.7deg_d	0.69	−1.02	−0.33
2P	16 deg	0.2π	1.29	19.3deg_d	0.152	18.7deg_d	0.44	19.1deg_d	0.68	−0.89	−0.21
2P	8 deg	-0.46π	1.41	18.9deg_d	0.159	19.3deg_d	0.46	19.4deg_d	0.00	−0.60	−0.60
2P	8 deg	-0.16π	1.49	19.4deg_d	0.184	18.8deg_d	0.49	19.2deg_d	0.22	−0.81	−0.59
2P	8 deg	0.09π	1.39	19.4deg_d	0.172	18.8deg_d	0.47	19.1deg_d	0.54	−0.79	−0.25
2P	8 deg	0.27π	1.33	19.0deg_d	0.156	19.2deg_d	0.45	19.4deg_d	0.42	−0.71	−0.29
3P	16 deg	-0.5π	1.53	19.1deg_d	0.173	18.4deg_d	0.48	18.8deg_d	0.33	−0.77	−0.43
3P	16 deg	-0.25π	1.51	18.5deg_d	0.151	19.1deg_d	0.45	19.3deg_d	0.20	−0.77	−0.56
3P	16 deg	-0.06π	1.53	19.7deg_d	0.173	19.3deg_d	0.50	19.5deg_d	0.44	−0.85	−0.41
3P	8 deg	-0.46π	1.41	19.3deg_d	0.172	18.8deg_d	0.47	19.1deg_d	0.23	−0.68	−0.45
3P	8 deg	-0.2π	1.41	18.9deg_d	0.156	19.1deg_d	0.45	19.4deg_d	0.29	−0.77	−0.48
3P	8 deg	-0.07π	1.47	19.6deg_d	0.177	19.2deg_d	0.49	19.4deg_d	0.34	−0.71	−0.37
4P	16 deg	-0.5π	1.41	18.3deg_d	0.197	19.2deg_d	0.50	19.4deg_d	0.28	−0.71	−0.42
4P	16 deg	-0.26π	1.43	19.5deg_d	0.154	19.0deg_d	0.46	19.3deg_d	0.11	−0.74	−0.63
4P	8 deg	-0.46π	1.41	19.3deg_d	0.172	19.1deg_d	0.47	19.4deg_d	0.26	−0.74	−0.48
4P	8 deg	-0.2π	1.44	19.3deg_d	0.168	18.7deg_d	0.47	19.1deg_d	0.26	−0.72	−0.46

[a]The subscript d denotes α during pitch-down.

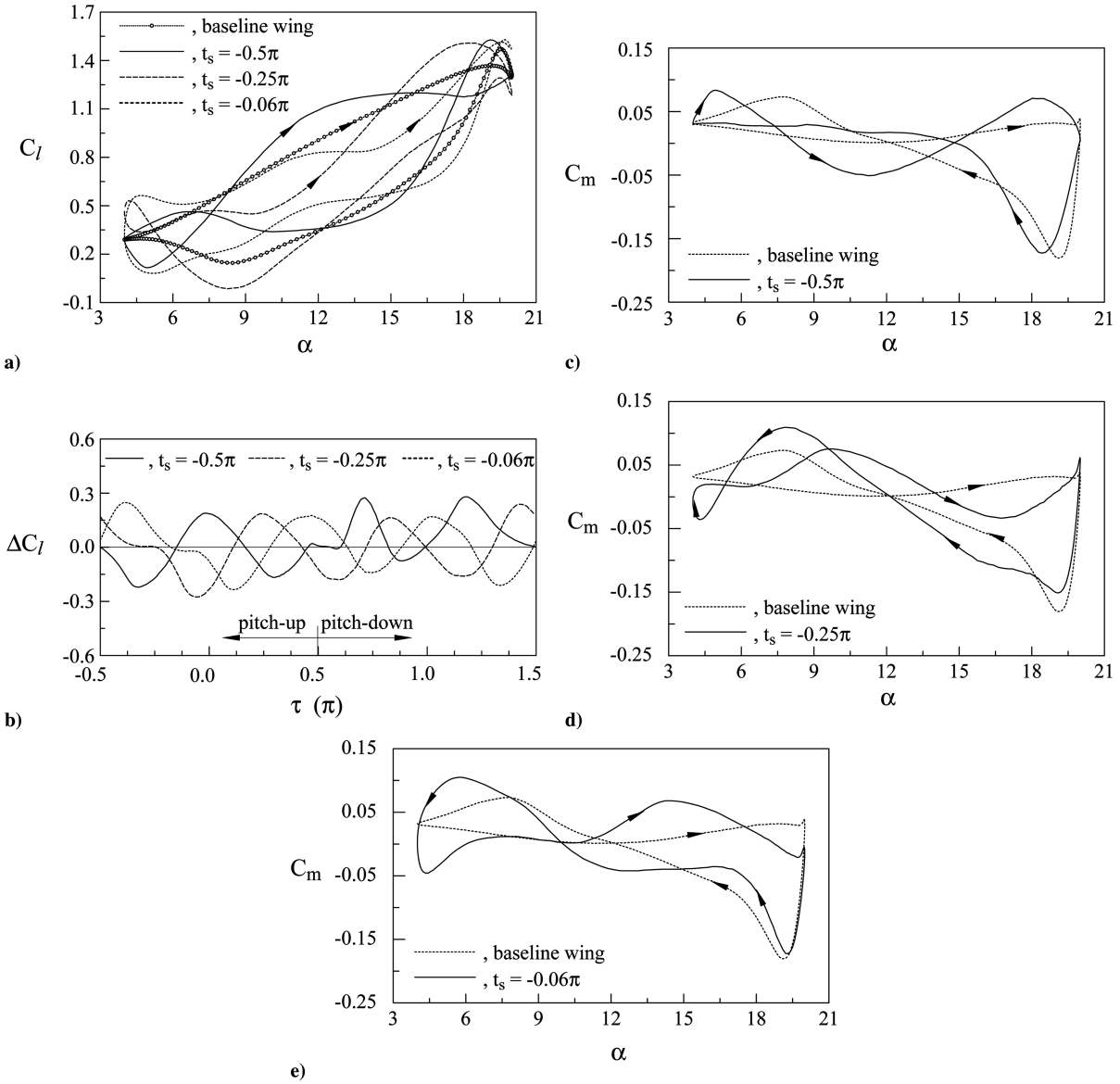

Fig. 7 Effect of 3P flap motion on C_l, ΔC_l, and C_m.

motions considered, the HHC flap motion only introduced a minor change in $C_d - \alpha$ loops and $C_{d,\max}$ (Table 1).

B. Effect of t_s and $\delta_{\max}$

The effect of the flap actuation start time and the peak-to-peak flap deflection (16 and 8 deg) on the dynamic C_l and C_m loops was also investigated and is presented in Figs. 5–8 and Table 1. For a 2P flap control, four different t_s (-0.46, -0.15, 0, and 0.20π, corresponding to a flap actuation at $\alpha_u = 4$, 8.4, 12, and 16.9 deg, respectively, with $\delta_{\max} = 16$ deg) were tested. The later the 2P flap actuation, the higher the net torsional damping $C_{w,\text{net}}$, with both $C_{w,\text{ccw}}$ and $|C_{w,\text{cw}}|$ increased with t_s (Fig. 6). The value of $|-C_{m,\text{peak}}|$ was, however, increased with increasing t_s. For $t_s > -0.5\pi$ (Fig. 5a), the $C_{l,\max}$ was increased (above the baseline-wing value) with t_s (reaching a local peak at $t_s = -0.15\pi$) and started to decrease with increasing t_s. The lowest $C_{l,\max}$ of 12% reduction was observed for a 2P flap deflected at $t_s = 0.2\pi$. Note that for a 2P flap deflected at $t_s = 0.20\pi$ or $\alpha_u = 16.9$ deg (i.e., near the end of the upstream propagation of the flow reversal and the onset of LEV formation [18]), the magnitudes of $C_{l,\max}$, $C_{d,\max}$, and $C_{m,\text{peak}}$ were 12, 16, and 12% below those of a baseline wing. On the other hand, the $t_s = -0.15\pi$ case was found to provide the highest $C_{l,\max}$, $|-C_{m,\text{peak}}|$, and $|C_{w,\text{net}}|$. The C_p and wake flow measurements also indicate that regardless of t_s, the phase angles at which the formation and detachment of the LEV occur were found to be virtually unaffected by the TEF motion. The low-pressure signature or footprint of the LEV was, however, reduced by the flap deflection (compared with a baseline wing), except in the trailing-edge region (Fig. 3c and 3d). The variation in ΔC_l with t_s was also obtained and is presented in Fig. 5b. Note that for clarity, the ΔC_l values were plotted as a function of τ instead of the conventional $C_l - \alpha$ representation. Note that the sign of ΔC_l not only indicates the increase or decrease of the C_l values (compared with a baseline wing) in response to the flap motion, but also suggests the increase or decrease in the C_l hysteresis (i.e., negative and positive ΔC_l values during pitch-up and pitch-down, respectively, reflecting a reduced C_l hysteresis).

The variation of C_l, C_m, ΔC_l, C_w, and $-C_{m,\text{peak}}$ with t_s (-0.5, -0.25, and -0.06π) and $\delta_{\max}$ of 3P flap deflection is depicted in Figs. 6 and 7. With $\delta_{\max} = 16$ deg, there was a minor improvement in $C_{l,\max}$ and $C_{m,\text{peak}}$ (Figs. 7a and 7c–7e), accompanied by a decreased $C_{w,\text{cw}}$, in comparison with the baseline-wing data. The net C_w or $C_{w,\text{net}}$ values were found to remain unchanged, except for the $t_s = -0.25\pi$ case. The change in the dynamic C_l values (compared with a baseline wing) as a function of the phase angle over an entire oscillation cycle is summarized in Fig. 7b. The $t_s = -0.06\pi$ case (i.e., a 3P flap deflection started near α_m or the onset of flow reversal) rendered a substantially decreased C_l hysteresis and $C_{w,\text{cw}}$. The increase in $|C_{w,\text{cw}}|$ was compensated by an improved $C_{w,\text{ccw}}$ and thus rendered an unchanged net C_w value, compared with a baseline wing. Special attention should be given to the increase in C_l during the poststall flow condition (compared with a baseline wing), preceded by a prestall lift loss during the upstream propagation of the flow reversal point (i.e., for $\alpha_u = \alpha_m$ to around 18 deg) for the $t_s = -0.06\pi$ and $\delta_{\max} = 16$ deg cases. Among the three flap start times tested, the $t_s = -0.25\pi$ control case rendered the lowest $|-C_{m,\text{peak}}|$, but the highest net negative damping or $C_{w,\text{net}}$ (Table 1 and Fig. 6). Table 1 also indicates that (in contrast to an improved $C_{l,\max}$ for the $\delta_{\max} = 16$ deg control case) a lowered $C_{l,\max}$ was observed for the $\delta_{\max} = 8$ deg case. No significant variation in the values of $-C_{m,\text{peak}}$, $C_{w,\text{cw}}$, $C_{w,\text{ccw}}$, and $C_{w,\text{net}}$, however, was noticed with reduced flap deflection.

The effect of t_s and $\delta_{\max}$ of 4P flap motion on the dynamic-load loops was also investigated (Figs. 8a–8c). In contrast to the 2P and 3P flap control (with $t_s \approx -0.5$ and -0.26π), the 4P flap motion always rendered a reduced $C_{l,\max}$ (compared with a baseline wing), regardless of t_s and $\delta_{\max}$. Also, similar to the 3P case, the earlier the flap actuation, the higher $|-C_{m,\text{peak}}|$ (above the baseline-wing value), whereas the $C_{w,\text{net}}$ was not affected. A delayed flap deflection, however, rendered a significantly reduced $|-C_{m,\text{peak}}|$ and $C_{w,\text{net}}$; a 15% improvement in $C_{m,\text{peak}}$, associated with a 58 and 50% reduction

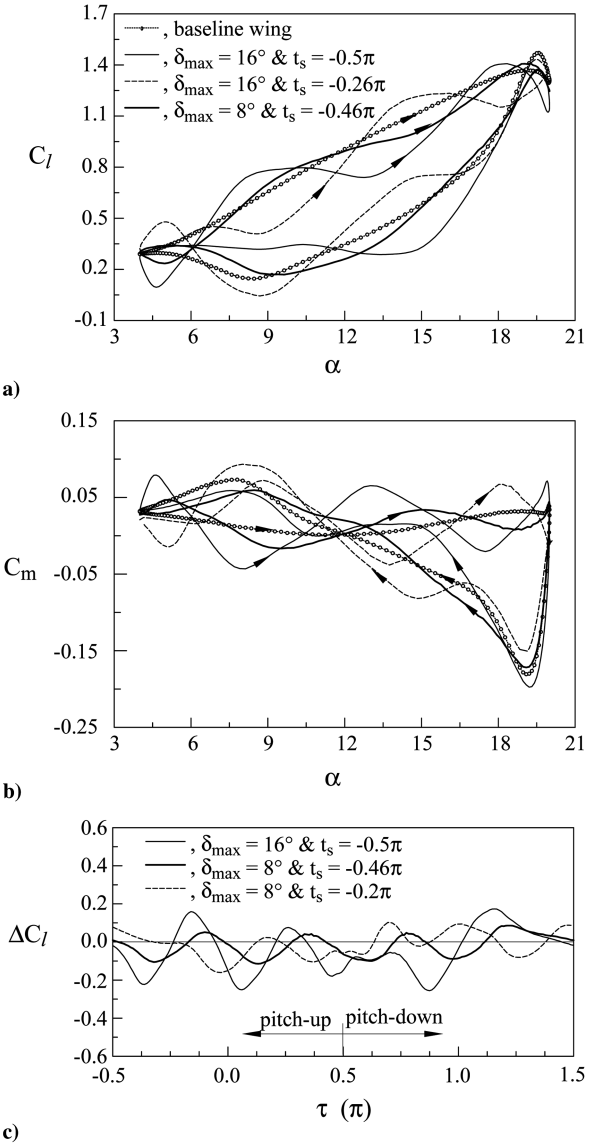

Fig. 8 Effect of 4P flap motion on C_l, ΔC_l, and C_m.

in $C_{w,\text{ccw}}$ and $C_{w,\text{net}}$, respectively (compared with a baseline wing), was observed for a 4P flap motion actuated at $t_s = -0.26\pi$ with $\delta_{\max} = 16$ deg. The results also show that for 4P flap control with $\delta_{\max} = 8$ deg,

1) There was always a minor improvement in $C_{m,\text{peak}}$, in contrast to the $\delta_{\max} = 16$ deg case.

2) The $C_{w,\text{ccw}}$ value remained unchanged.

3) No significant change in $C_{w,\text{ccw}}$ and $C_{w,\text{net}}$ was observed, compared with a baseline wing.

4) The later the flap actuation, the lower $|-C_{m,\text{peak}}|$. In addition, no noticeable difference in $C_{l,\max}$ and $C_{d,\max}$ was observed between the two $\delta_{\max}$ tested.

IV. Conclusions

The effects of prescheduled HHC flap motions on the dynamic C_l and C_m values of an oscillating NACA 0015 wing were investigated. At fixed t_s and $\delta_{\max}$, the 2P flap deflection provided a significant alleviation of $-C_{m,\text{peak}}$ and the lowest $C_{w,\text{net}}$, compared with a baseline wing with and without 3P and 4P flap control. The 3P flap motion rendered a reduced nose-down C_m, a slightly increased $C_{l,\max}$, and a virtually unchanged $C_{w,\text{net}}$, compared with 4P flap control. The 4P flap control provided the lowest $C_{l,\max}$ and the highest $-C_{m,\text{peak}}$ among the three NP tested. Only a minor change in $C_d - \alpha$ loops and $C_{d,\max}$ was observed for all the flap motions tested.

The formation and spillage of the LEV was generally unaffected. For HHC flap motions deflected at different t_s, the results show that the later the 2P flap actuation, the higher the net torsional damping and the lower $C_{m,\text{peak}}$. For 3P flap control, a minor improvement in $C_{l,\max}$ and $C_{m,\text{peak}}$, accompanied by a decreased $C_{w,\text{cw}}$, regardless of t_s (in comparison with the baseline-wing data), was observed; the net C_w or $C_{w,\text{net}}$ values were found to remain unchanged, except for the $t_s = -0.25\pi$ flap control case. Finally, in contrast to the 2P and 3P flap deflected at the same t_s, the 4P flap motion always rendered a reduced $C_{l,\max}$, regardless of t_s and $\delta_{\max}$. Also, the earlier the flap actuation, the higher $|-C_{m,\text{peak}}|$, with $C_{w,\text{net}}$ unaffected.

Acknowledgment

This work was supported by the Natural Science and Engineering Research Council (NSERC) of Canada.

References

[1] McCroskey, W. J., "Unsteady Airfoils," *Annual Review of Fluid Mechanics*, Vol. 14, 1982, pp. 285–311.

[2] Rennie, R., and Jumper, E. J., "Experimental Measurements of Dynamic Control Surface Effectiveness," *Journal of Aircraft*, Vol. 33, No. 5, 1996, pp. 880–887.

[3] Vipperman, J. S., Clark, R. L., Conner, M., and Dowell, E. H., "Experimental Active Control of a Typical Section Using a Trailing-Edge Flap," *Journal of Aircraft*, Vol. 35, No. 2, 1998, pp. 224–229.

[4] Ekaterinaris, J. A., "Numerical Investigations of Dynamic Stall Active Control for Incompressible and Compressible Flows," *Journal of Aircraft*, Vol. 39, No. 1, 2002, pp. 71–78.

[5] Feszty, D., Gillies, E. A., and Vezza, M., "Alleviation of Airfoil Dynamic Stall Moments Via Trailing-Edge-Flap Flow Control," *AIAA Journal*, Vol. 42, No. 1, 2004, pp. 17–25.

[6] Gerontakos, P., and Lee, T., "Dynamic Stall Flow Control Via a Trailing-Edge Flap," *AIAA Journal*, Vol. 44, No. 3, 2006, pp. 469–480.

[7] Smith, B. L., and Glezer, A., "The Formation and Evolution of Synthetic Jets," *Physics of Fluids*, Vol. 10, No. 9, 1998, pp. 2281–2297.

[8] Wygnanski, I., and Greenbaltt, D., "Dynamic Stall Control by Periodic Excitation, Part 1: NACA 0015 Parametric Study," *Journal of Aircraft*, Vol. 38, No. 3, 2001, pp. 430–438.

[9] Karim, M. A., and Acharya, M., "Suppression of Dynamic-Stall Vortices over Pitching Airfoils by Leading-Edge Suction," *AIAA Journal*, Vol. 32, No. 8, 1994, pp. 1647–1655.

[10] Chandrasekhara, M. S., and Wilder, M. C., "Unsteady Stall Control Using Dynamically Deforming Airfoils," *AIAA Journal*, Vol. 36, No. 10, 1998, pp. 1792–1800.

[11] Payne, P. R., "Higher Harmonic Rotor Control," *Aircraft Engineering*, Vol. 30, No. 354, 1958, pp. 222–226.

[12] Ham, N. D., "Some Conclusions from an Investigation of Blade Vortex Interaction," *Journal of the American Helicopter Society*, Vol. 20, No. 4, 1975, pp. 26–31.

[13] Wood, E. R., Powers, R. W., and Hammond, C. E., "On Methods for Application of Harmonic Control," *Vertica*, Vol. 4, No. 1, 1980, pp. 43–60.

[14] Wood, E. R., Powers, R. W., Hammond, C. E., and Cline, J. H., "On Developing and Flight Testing a Higher Harmonic Control System," *Journal of the American Helicopter Society*, Vol. 30, No. 1, 1985, pp. 3–20.

[15] Shaw, J., Albion, N., Hanker, E. J., and Teal, R. S., "Higher Harmonic Control: Wind Tunnel Demonstration of Fully Effective Vibratory Hub Force Suppression," *Journal of the American Helicopter Society*, Vol. 34, No. 1, 1989, pp. 14–25.

[16] Straub, F. K., "Development of a Piezoelectric Actuator for Trailing-Edge Flap Control of Full Scale Rotor Blades," *Smart Materials and Structures*, Vol. 10, No. 4, 2001, pp. 25–34.

[17] Enenkl, B., Kloppel, V., Preibler, D., and Janker, P., "Full Scale Rotor with Piezoelectric Actuated Blade Flaps," *28th European Rotorcraft Forum*, Royal Aeronautical Society, London, 2002.

[18] Lee, T., and Gerontakos, P., "Investigation of Flow over an Oscillating Airfoil," *Journal of Fluid Mechanics*, Vol. 512, Aug. 2004, pp. 313–341.